SEISMIC TESTING OF MODEL-SCALE GEOSYNTHETIC-REINFORCED SOIL WALLS

Perry Jackson[1], Elisabeth T. Bowman[1], Misko Cubrinovski[1]

SUMMARY

This paper presents an experimental study on a series of reduced-scale model GRS walls with Full-Height-Rigid facings conducted on a shake-table at the University of Canterbury. Each model was 900 mm high, reinforced by five layers of stiff Microgrid reinforcement and constructed of dry dense Albany sand. The ratio of geogrid length L to wall height H, L/H, was varied from 0.6 to 0.9, while the wall inclination was generally vertical (90° to horizontal) with 70° for one test. During sinusoidal shaking, facing displacements and accelerations within the backfill were recorded. Failure for all models was predominantly by overturning, with some small sliding component generated in the final shaking step. An increase in L/H resulted in a decrease in wall displacement, while a decrease in wall inclination from the vertical resulted in similar benefits. Detailed analysis of the deformation of one of the tests is presented. During testing, global and local deformations within the backfill were investigated using two methods: the first utilised coloured horizontal and vertical sand markers placed within the backfill; the second utilised high-speed camera imaging for subsequent analysis using Geotechnical Particle Image Velocimetry (GeoPIV) software. GeoPIV enabled strains to be identified within the soil at far smaller strain levels than that rendered visible using the coloured sand markers. These complementary methods allowed the spatial and temporal progressive development of deformation within the reinforced and retained backfill to be examined.

INTRODUCTION

Reinforced soil systems enable shortened construction time, lower cost, improved seismic performance and aesthetic benefits over their conventional counterparts, such as gravity and cantilever type retaining walls [1, 2, 3, 4]. Further, soil reinforcement meets many of the goals associated with sustainable development, such as reduced carbon emissions and embodied energy, in addition to cost reductions noted when compared to conventional type retaining walls [1, 5].

This paper presents an experimental study on the seismic performance of Geosynthetic Reinforced Soil (GRS) retaining walls. The study consisted of a series of 1-g shake-table tests on reduced-scale models of GRS walls conducted on the University of Canterbury shake-table. The models were faced with a Full-Height Rigid (FHR) panel. Two key parameters that influence seismic behaviour, namely the reinforcement length to height ratio (L/H), and the wall inclination (α), were varied systematically during testing. Facing displacements, accelerations within the backfill, and backfill deformations were recorded during each test.

Global and local deformations within the backfill were of particular interest and were investigated using a combination of sand markers, and high-speed camera imaging and subsequent analysis using the Geotechnical Particle Image Velocimetry (GeoPIV) methodology [6]. GeoPIV allowed in-depth observations and analyses of strain fields to be made for selected regions of the retained soil and backfill.

BACKGROUND

Use of GRS walls in New Zealand

Design of GRS walls in New Zealand uses several different overseas standards and design guidelines, i.e. Federal Highways Administration (FHWA 2001), British Standards Institute (BS8006:1995), Australian Standards (AS4678-2002), and the Deutsches Institut Bautechnik (DIBt). Manufacturers of geosynthetic reinforcement such as Tensar and Stratagrid, also produce design methods and guidelines. Hence, GRS structures in New Zealand have been built with varying resistance to static and seismic loads, and thus different seismic risk [7].

To address this uncertainty, in 1998 Murashev [7] prepared guidelines for the design and construction of GRS walls in New Zealand, as commissioned by Transfund New Zealand (now part of the New Zealand Transport Agency). The guidelines are based on a limit state approach and are a combination of design methods and research for the New Zealand context. Murashev [8] also surveyed a majority of GRS structures constructed in New Zealand up to 1998, which included some 54 structures, built predominantly for road applications, which ranged in wall height from 2 m to 13 m. The study took into account roughly an equal number of walls and slopes (a slope is defined as being at an inclination of less than 70^o to the horizontal). Murashev found the predominant method of facing for GRS structures in New Zealand to use wrap-around technology, reflecting the relatively low structural performance required of minor State Highways and rural roads.

Worldwide, case histories demonstrate that GRS structures have performed well in earthquakes, especially in comparison

[1] *Department of Civil and Natural Resources Engineering, University of Canterbury, Christchurch, New Zealand*

to conventional retaining walls. However, it should be noted that there have been some limited cases where large deformation and/or failure of GRS Segmental Retaining Walls (SRW) and those constructed with wrap-around facings have occurred, for example in the Northridge and Chi-Chi earthquakes of 1994 and 1999, respectively [9,10].

Between late 2010 and mid 2011, the Canterbury region was devastated by a series of shallow earthquakes of magnitude 7.1, 6.3 and 6.1 occurring in September 2011, February 2012 and June 2012, respectively. Observations of geosynthetic reinforced structures after the first of these earthquakes indicated that they performed relatively well [11, 12]. For example, a gabion faced wall located in the Cashmere Hills was reported to have suffered only minor settlements and wall movements well within the design limits of the structure, even though the estimated horizontal peak ground acceleration of 0.3g at the site likely exceeded the structure's design acceleration [11]. During the February 2012 earthquake however, the horizontal peak ground acceleration was estimated to be up to 3 times higher – between 0.8 and 0.9g – which resulted in further fill settlements and gabion rotation of up to 200 mm, however no catastrophic failure occurred [11]. Field observations post-February 2012 of a Mechanically Stabilised Earth wall (MSE) as part of the Southern Motorway extension (one wall completed, one mid-construction) found that no damage was evident [12].

The authors' own observations made during 3 months of extensive field work from June 2012, indicated that no GRS walls failed catastrophically, although serviceability was sometimes compromised. An example of a gabion basket faced reinforced soil wall in the Cashmere Hills, up to 4 m high, is shown in Figure 1. This particular wall suffered fill settlements of up to 300 mm, and overturning and bulging of a similar order, while a single gabion basket had bulged open. The wall did not collapse.

Figure 1: Gabion basket wall, Cashmere Hills.

In general, the observed gabion basket walls exhibited rotation at the wall top, bulging, and minor sliding damage, but no collapse. In contrast, some collapses of timber crib walls and severe cracking/spalling of reinforced concrete walls was found.

Case histories show that GRS walls with Full-Height Rigid (FHR) facing perform better than other GRS wall types [1, 9, 10] producing less deformation under seismic load. Accordingly, Japan, which is seismically active, has adopted the use of FHR GRS walls as standard technology for vulnerable lifeline assets such as high-speed railways [1].

To the authors' knowledge, to date in New Zealand there has been little to no use of FHR facing for GRS walls. However, this position is likely to change in the near future as requirements for seismic performance of key geotechnical structures are increased and as confidence in the technology is gained. Accordingly this paper focuses on the behaviour of FHR walls under seismic loading.

Previous testing on GRS scale models

1-g tests

A number of 1-g shake-table studies on scaled-down GRS models have been conducted previously, such as El-Emam and Bathurst [3, 13, 14], Watanabe *et al.* [15], and Sabermahani *et al.* [16].

El-Emam and Bathurst [3, 13, 14] conducted a series of 1 m high reduced-scale GRS model tests with FHR panel facing on a shake-table. The models incorporated a scaled geosynthetic geogrid with sand glued to its surface to ensure good soil-reinforcement interlock. Parameters such as L/H ratio, reinforcement spacing and stiffness, and facing inclination and mass were investigated. The models were subjected to incrementally increasing sinusoidal base shaking until model failure. In general, an increase in the L/H ratio from 0.6 to 1.0, a decrease in wall inclination from the vertical, and a decrease in facing mass each resulted in a decrease in the displacement accrued before failure, and an increase in the acceleration at which failure occurred. Observed failure modes included sliding and overturning, however the actual mechanisms of deformation within the backfill were not observed.

Watanabe *et al.* [15] conducted 0.5 m high reduced-scale model shake-table tests on both conventional (gravity, cantilever and leaning type retaining walls) and GRS walls with vertical FHR facing (L/H = 0.4 and 0.7, and reinforcement spacing = 50 mm), this time with a transparent sidewall, and horizontal layering of dyed sand within the soil deposit so that deformation mechanisms could be observed. Of interest, at low shaking amplitudes, the GRS walls were found to deform more than the conventional-type retaining walls, but they were able to sustain far higher shaking levels prior to failure. During shaking, as the wall face tilted outwards, the progressive development of two inclined failure surfaces extending from the back of the reinforced soil block upwards into the retained backfill, as well as a near-vertical failure surface tracing the back of the reinforced soil block was observed. At ultimate failure, the lowest failure surface was visible from the bottom layer of reinforcement and upwards back into the retained backfill. No inclined failure surfaces were observed within the reinforced block, indicating sufficient reinforcement to prevent such deformation. Overturning was observed as the dominant failure mode, which accompanied simple shearing within the reinforced soil block itself between reinforcement layers.

Sabermahani *et al.* [16] tested 1.0 m high vertical walls with a wrap-around facing (L/H = 0.5 to 0.9, reinforcement spacing = 100 mm to 200 mm), on a shake-table. Overturning failure was accompanied by multiple failure surfaces which formed in the backfill and extended down to the second or third layer of reinforcement (from model base). Bulging of the wall face occurred for GRS walls using reinforcement of very low stiffness or large reinforcement spacing, and resulted in the largest displacement being recorded around mid-height of the face (and not at the wall top as in overturning failure). This failure mode was accompanied by an internal slip surface along the soil-reinforcement interface within the reinforced soil block.

Centrifuge testing

The use of the centrifuge enables prototype stresses at depth to be properly scaled, which may influence the development of failure mechanisms, for example by inducing a more ductile

response under higher confining pressure. Accordingly, seismic centrifuge tests on GRS walls and slopes have been conducted by several researchers. These studies have focused on flexible front facings - e.g. Nova-Roessig and Sitar [17], who used wrap-around facing and Izawa and Kuwano [18] who used segmental facing. The results indicate that distinct failures surfaces may be suppressed at high g, although how this influences the load-displacement response of the structure is unclear.

To the authors' knowledge, no study has been published to date of centrifuge tests using FHR facing, although that of Howard *et al.* [19] may come closer than most. In this study the models were faced by wide, discrete panels, and with this experimental set-up, clear failure surfaces were visible in one model of short L/H = 0.5 ratio. Hence while for GRS walls in general, a more ductile response may occur under higher confining pressure (for example, at full-scale), the influence of facing may be of greater importance.

FHR facing design consideration

These observations highlight the importance of facing type, inclination, reinforcement layout and material properties on GRS seismic behaviour and the mechanisms of deformation. An FHR panel facing appears to constrain the formation of failure surfaces associated with ultimate failure to the heel of the reinforced soil block [1], as shown in Figure 2, whereas for non-rigid faced walls, it is likely that the wrap-around faced models fail before the bottom most layer of reinforcement can be sufficiently engaged to resist deformation. Further, depending on reinforcement arrangement and relative soil-reinforcement stiffness, failure surfaces may form within the reinforced soil block itself.

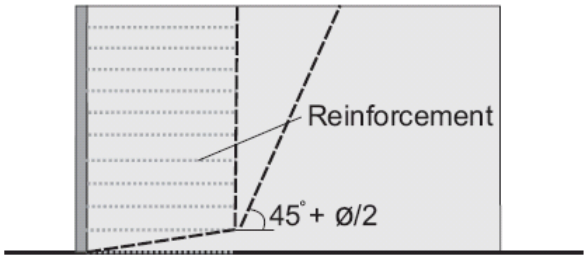

Figure 2: Two-wedge failure mechanism used in Japanese design. Redrawn after Tatsuoka [1].

Use of image tracking in GRS model wall tests

For the purposes of non-intrusive measurement in geotechnical engineering applications, Particle Image Velocimetry (PIV) techniques have been used to identify displacements and shear strains within retaining wall models tested in a centrifuge [18, 20] and on a shake-table [21, 22]. These tests arrangements used sand markers placed in a grid pattern throughout the backfill and/or a wide-angle view of the full test, allowing a relatively coarse examination of strain to be undertaken.

The GeoPIV software for geotechnical engineering applications developed and described by White *et al*. [23] is the particular technique used in the experiments presented herein. In contrast to using sand markers, GeoPIV utilises sand texture, (the pattern of varying brightness of soil particles), to identify and trace soil displacements via images taken at the sides of a physical model test. This enables far more detailed strains to be determined in comparison to methods using sand markers. Specifically, the tests here used cameras placed at zones of particular interest and expected high strain development - namely at the ends of the reinforced soil zone and within the reinforced soil, focussing on a particular reinforcement layer. This enabled a highly detailed examination of local strain development to be made and linked to the global response. Appendix 1 presents details of the GeoPIV technique used.

EXPERIMENTAL DESIGN

Scale Model Design

Previous scale model shake-table testing was reviewed in order to determine appropriate strong-box dimensions. The model/box geometry and construction material details used in some recent 1-g shake table studies are summarised in Table 1.

Appropriate scaling is important when conducting scale model tests to ensure the behaviour observed at model scale is representative of behaviour at full scale. Hence the size of the wall and material components, such as facing, reinforcement, and soil were selected based on the scaling rules suggested by Iai [24] to satisfy geometric, dynamic and kinematic similitude. Shake-table and material limitations resulted in a geometric scale of 1:5 selected to model a 4.5 m high wall at prototype scale.

A strong-box dimensioned 1,100 mm high, 800 mm wide and 3,000 mm long was constructed of steel with an internal plywood base coated with a layer of glued sand to ensure sufficient friction between the rigid base and backfill. One of the sides was constructed with 20 mm thick transparent Perspex and reinforced at 200 mm intervals. The model dimensions as well as the typical instrumentation layout used in each test are shown in Figure 3. Instrumentation included four accelerometers within the backfill (Acc2-Acc5), and two

Table 1: Summary of previous studies model geometry and materials, including this study.

Reference	Scale	Box dimensions L, W, H (m)	Model height (m)	Construction materials
Sabermahani *et al*. [16]	1:5	1.8, 0.8, 1.2	1.0	Rigid Plexiglass
El-Emam and Bathurst [3, 13, 14]	1:6	2.4, 1.0, 1.0	1.0	Steel lined with plywood and a glued sand base layer
Watanabe *et al.* [15]	1:10	2.6, 0.6, 1.4	0.5	Steel and plexiglass. Greased Teflon used on side of model wall
Matsuo *et al*. [26]	1:3	4.0, 0.9, 2.0	1.5	Steel with sand paper glued to base
This study [25]	1:5	3.0, 0.8, 1.1	0.9	Steel lined with plywood and a glued sand base layer with transparent acrylic 20 mm thick side window

others to record the input motion at the base and top of the rigid box (Acc1 and Acc6); six displacement transducers in two arrays of three were positioned at the front of the wall (Disp1-Disp3, and Disp4-Disp6).

The wall face was a single FHR aluminium panel, 5 mm thick and 960 mm high, which fit into the 800 mm wide rigid box mounted onto a 4.0 m long by 2.0 m wide 1-D shake-table. (Note the extra 60 mm wall facing in height was to allow the same panel to be used for the inclined model wall test shown in Figure 3c). The backfill was Albany Sand compacted to a target relative density of Dr = 90% as discussed below. The sand was deposited upon the rigid box base with the glued sand layer.

Stratagrid Microgrid, a polyester geogrid was selected as the model reinforcement with an axial stiffness $J_{2\%}$ of 220 kN/m which corresponds to an equivalent stiffness of 5,500 kN/m at prototype scale. Hence whilst the microgrid is classified as 'extensible' under full-scale conditions, using Iai's [24] scaling considerations, within the prototype it is likely to behave more like an 'inextensible' reinforcement [25]. Five layers of geogrid, with a vertical spacing between layers of 150 mm was used for all models. The reinforcement length was varied to achieve a reinforcement-to-wall height ratio, L/H = 0.6, 0.75 and 0.9.

Model Construction

The models were constructed in stages. The Microgrid reinforcement was first attached to the facing panel, and a rigid connection was ensured. The panel was then lifted into the strong-box and braced into position prior to backfilling with Albany Sand.

The backfill was then constructed in layers 75 mm thick, and compacted by vibration of the shake-table – a similar process to that employed by El-Emam and Bathurst [3]. A known weight of sand (accurate to 200 grams) was deposited into the strong-box; this was then raked flat; next a 900 kg weight was placed on top of the layered sand; finally, the shake-table was vibrated for 10 seconds at a frequency of 12 Hz. The process was then repeated, interspersed with the careful placement of

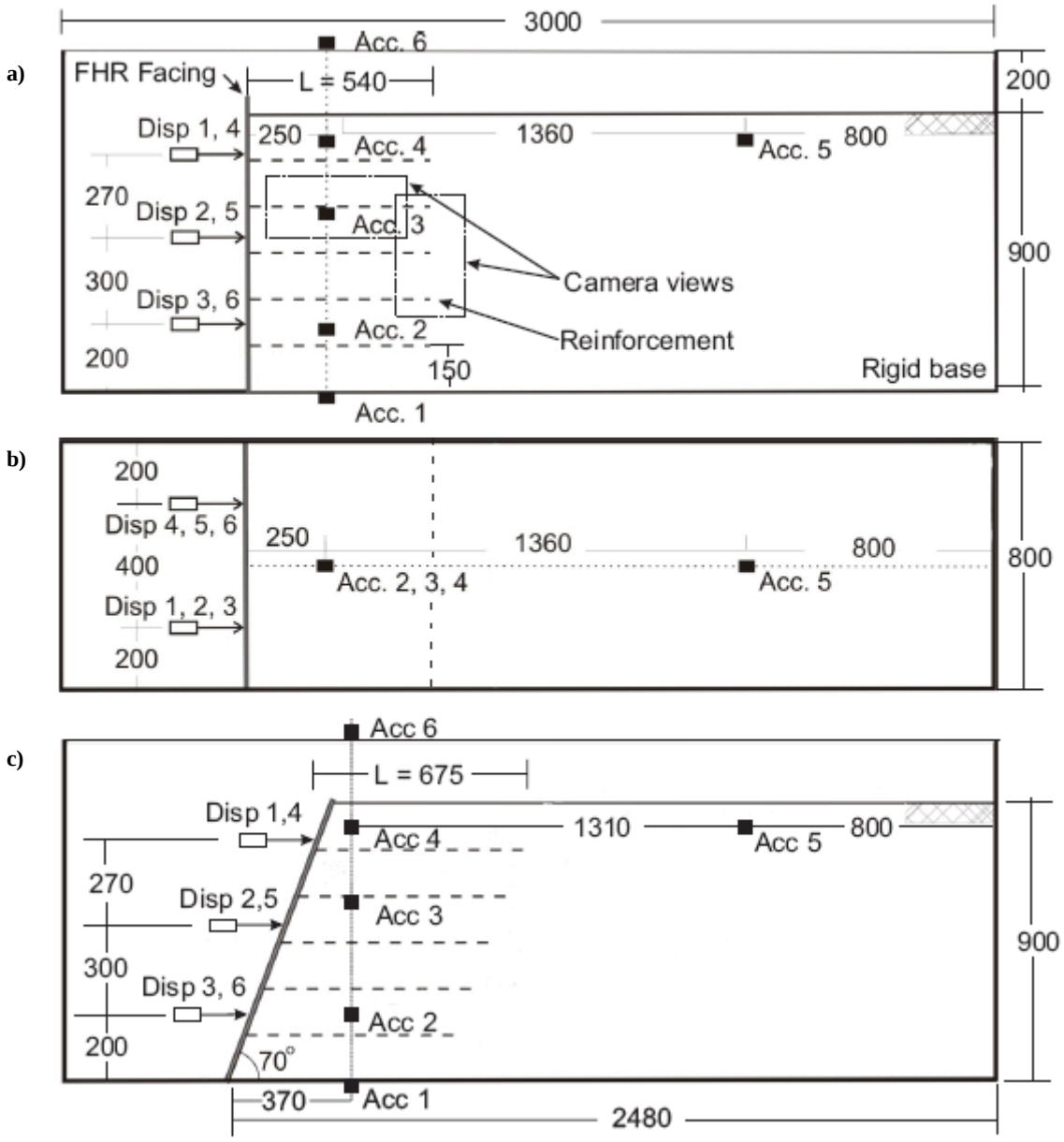

Figure 3: ***Model instrumentation for (a) the vertical wall reinforced the shortest at L/H = 0.6 (Test-2 and 6); (b) plan view of vertical wall and (c) the inclined wall reinforced by L/H = 0.75 (Test-7).***

the pre-attached reinforcement, the introduction of vertical and horizontal sand markers, and accelerometer instruments within the fill. Throughout the construction, the thickness of the sand deposit was measured at various locations so as to determine the deposit's relative density. For all tests a target relative density of approximately 90% was achieved.

A Teflon seal was utilised between the FHR panel wall and the side wall of the strong-box to reduce friction, and prevent leakage of the backfill around the side of the face during the high-frequency compaction vibration.

Model Testing

Following the scaling rules provided by Iai [24], and considering the frequency characteristics of strong ground motions, a sinusoidal wave with frequency of 5 Hz was adopted as a base excitation for the experiments. A frequency of 5 Hz was significantly lower than the fundamental frequency of the model determined to be approximately 40 Hz by initial impact load testing.

Even though a sinusoidal motion contains more energy than an irregular time-history having the same PGA, it has the advantage of a simple and accurate control of its intensity (sine wave amplitude) and hence has much better repeatability in shake-table tests. Further, this allowed comparison of results with other model studies conducted at this frequency of excitation [3, 15].

The staged shaking procedure adopted during testing, as implemented in one of the tests (Test-6) is shown in Figure 4. Each shaking step lasted 10 seconds (i.e. 50 cycles), with approximately 15 minutes in between stages reserved for downloading images from the two high-speed cameras. Details of the set up of the cameras are provided later. From an initial acceleration of 0.1g, the acceleration of each shaking step was increased by 0.1g relative to the previous step until failure occurred (for Test-6, this was 0.5g).

MODEL PERFORMANCE DURING SHAKING

Summary of testing series

The testing series consisted of seven reduced-scale FHR faced GRS models. Four of those tests, which include different reinforcement L/H ratios and inclination of the FHR facing are presented herein, as summarized in Table 2.

For all tests failure was triggered at a base acceleration between 0.5g and 0.7g. In order to demonstrate the typical failure pattern of the models, one of the tests, Test-6, is examined in detail in the following section. Note that the results of tests on the inclined wall model, Test-7, have been discussed in a previous paper that focussed on the development of localised strains [27] using GeoPIV.

Table 2: Summary of parameters varied during each test

Test	L/H ratio	Wall angle (^{o})	Acceleration at failure (g)
Test-1*	0.75	90	0.6
Test-5	0.9	90	0.7
Test-6	0.6	90	0.5
Test-7	0.75	70	0.7

* Some small leakage of sand at panel-side wall interface.

General pattern of deformation

In Test-6, a vertical wall with GRS reinforcement ratio, L/H = 0.6 was used. This was the lowest of the L/H ratios used in the series of shake table tests. The backfill was 900 mm high and was constructed to an average relative density of 89%. The finished model prior to shaking, including vertical and horizontal lines of coloured sand, is shown through the transparent side window in Figure 5 (a), which also identifies the reinforced soil zone and retained backfill.

Figure 5 (b) shows the deformed model at the end of 0.5g shaking. A combined sliding and overturning failure mode can be readily observed (other failure modes such as bearing capacity, bulging and reinforcement rupture are precluded by the model design). Deformation is predominantly by overturning, with only some minor sliding of the wall along the rigid base of the strong box. Overturning consisted of the reinforced soil block rotating about the toe, generating simple shear deformation within the reinforced soil block and multiple external failure surfaces which formed behind the reinforced soil block into the retained backfill.

Discontinuities in the coloured horizontal and vertical sand markers were used to plot the progression of failure during testing. Generally differential displacement of around 2 mm

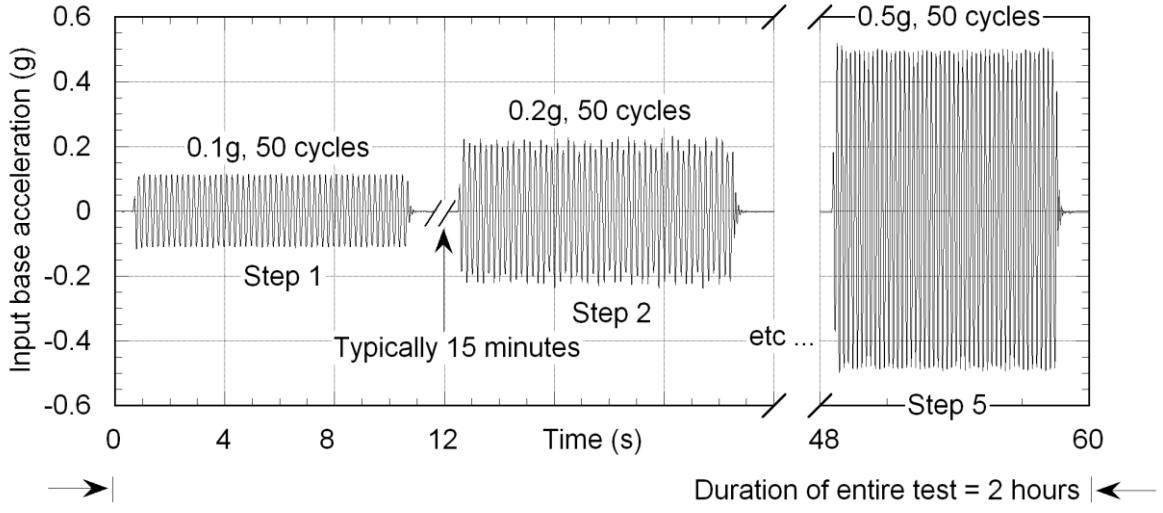

Figure 4: Staged testing procedure for Test-6.

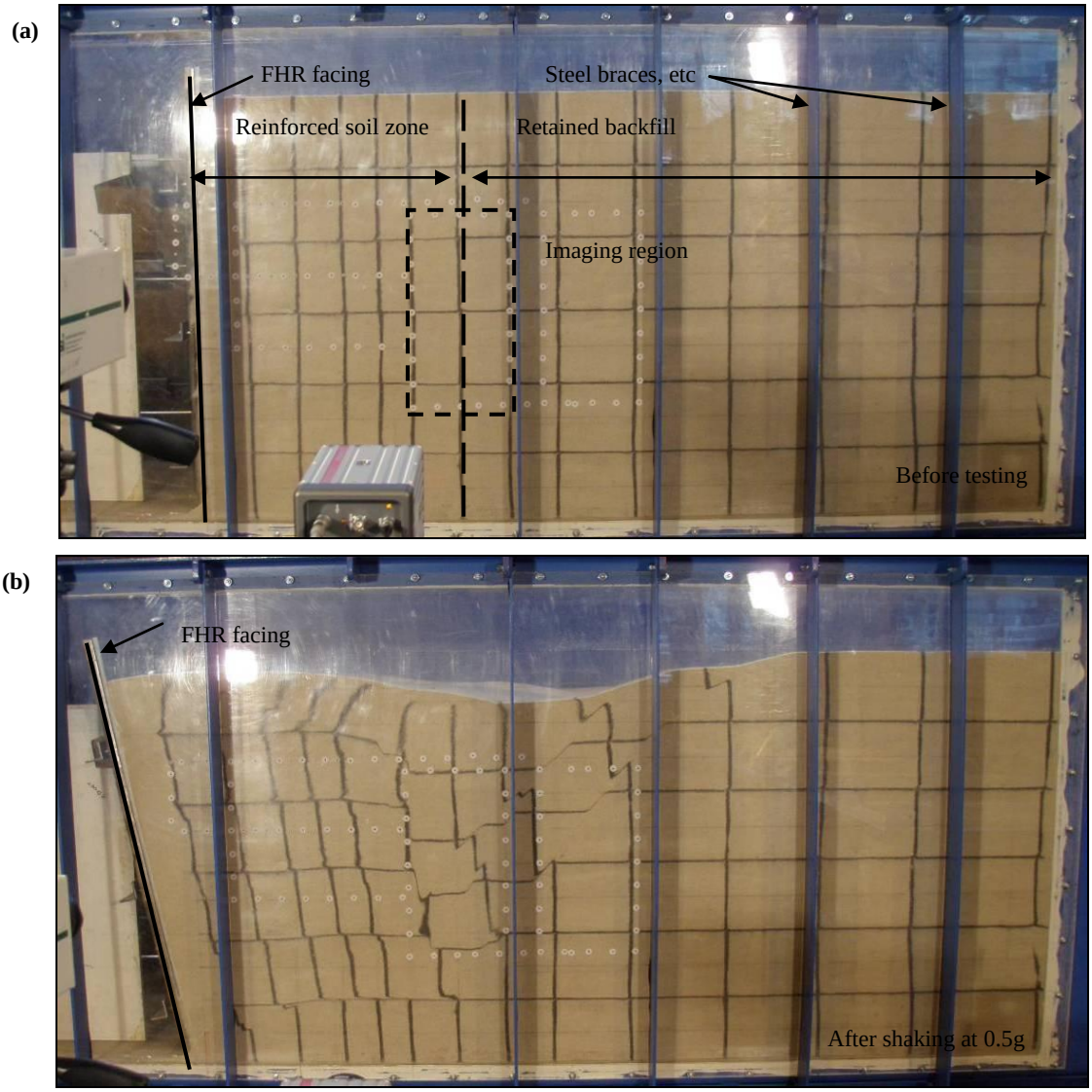

Figure 5: ***Test-6 (a) before shaking and (b) after shaking at 0.5g, during which failure occurred. The incorporation of black coloured vertical and horizontal lines allowed the deformation mechanisms to be clearly visible. Note that the intermediate stages of 0.2g, 0.3g and 0.4g are not shown.***

had to occur before a discontinuity became clear and was recorded based on this direct visual (naked eye) observation. The evolution of progressive failure surfaces within the reinforced and retained backfill with increasing shaking amplitude is shown in Figure 6, along with their orientations to the horizontal.

As illustrated in Figure 6, deeper failure surfaces generally formed with each subsequent (higher amplitude) shaking step. For instance, both the top-most inclined and sub-vertical failure surfaces were clearly visible after 0.3g base excitation; and these propagated downwards with further shaking. The deepest inclined failure surface formed only during the 0.5g shaking step. This general pattern is largely consistent with previous model testing [15, 16]. For example, for FHR facing models the deepest failure surface has been observed to intersect with the lowest layer of reinforcement [15], whereas for wrap-around faced walls, the deepest observed failure surface does not extend to the bottom layer of reinforcement [16]. This difference in behaviour shows the importance of facing type on seismic behaviour; a FHR panel facing ensures that all reinforcement layers are engaged and act in unison to resist deformation [1].

Measured wall displacements

Six displacement transducers arranged in two vertical arrays of three were used to measure displacement of the wall face (two arrays were used to check the plane strain condition; this was measured to be the case). Displacement recorded at the wall face was cyclic, and incorporated both recoverable and permanent displacements, as shown in Figure 7. For a given amplitude of shaking, each plot shows the displaced wall including its initial position, as well as the displacements after 5, 10, 20, 30, 40 and 50 cycles, and at the end of shaking.

It may be seen that constant amplitude cycles cumulatively contribute to the facing displacement at a relatively constant rate. It is also clear from the early stages of shaking that the displacement of the wall includes both sliding- and rotation-induced displacements. To better illustrate and quantify these displacements, the total displacement recorded at the top and bottom of the wall was used to attribute wall top displacement to either sliding or rotation (overturning) components (as illustrated in Figure 7), and is shown in Figure 8.

The total displacement-acceleration relationship is shown to be approximately bi-linear in Figure 8; typical of other physical model studies [3, 15]. At low base input accelerations, only a small amount of permanent deformation

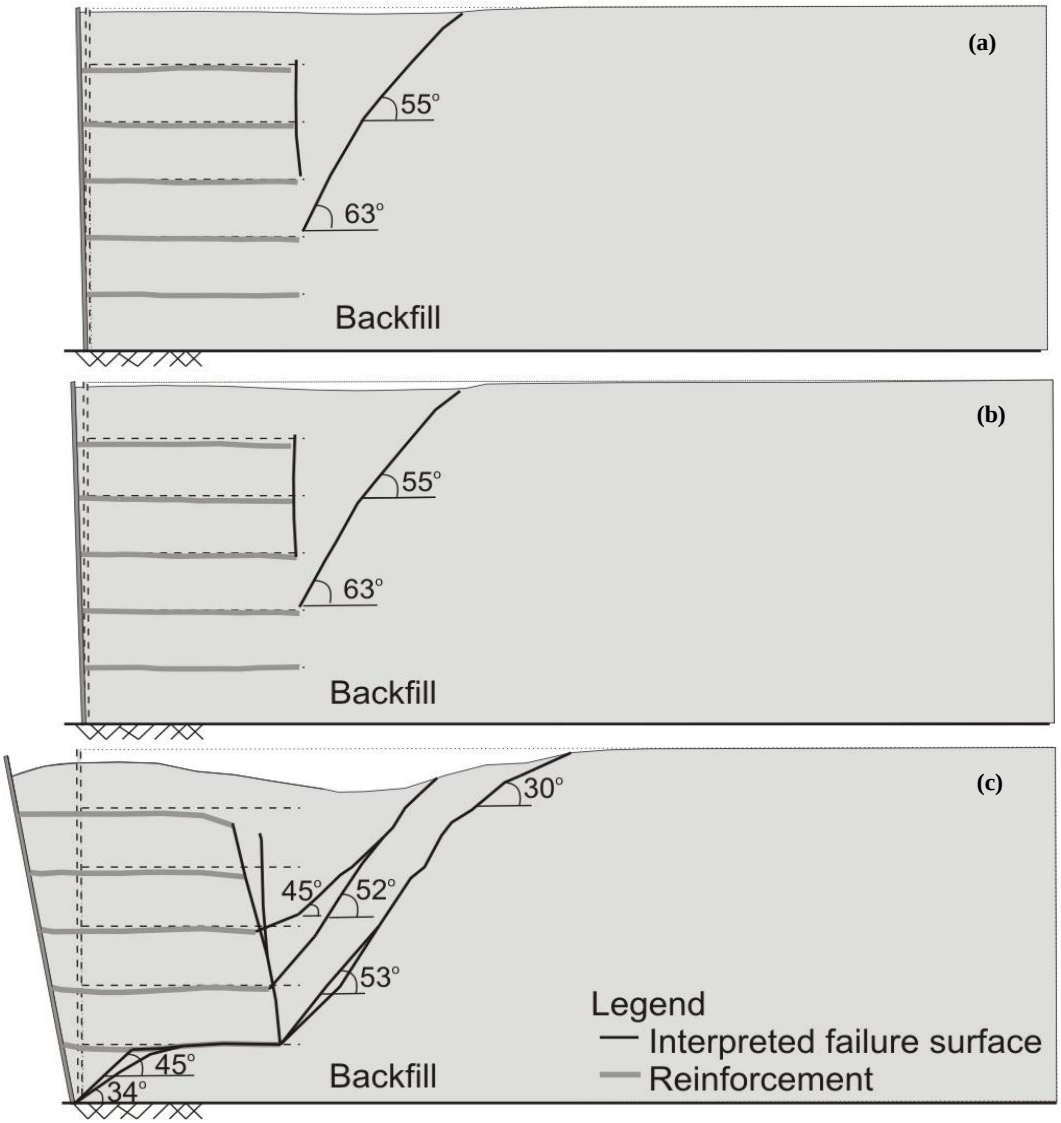

Figure 6: ***Interpretation of failure surfaces within the reinforced and retained backfill after the completion of (a) 0.3g, (b) 0.4g and (c) 0.5g shaking steps. (No discontinuities were clearly visible prior to 0.3g shaking).***

accrued; at base accelerations larger than some threshold value – in the above case, 0.4g – the rate of wall top displacement increased significantly until failure, where the physical limit of the strong-box was reached (i.e. where the wall reached the maximum displacement possible within the available space inside the rigid box). This threshold acceleration value can be considered as the model's critical acceleration value, above which shaking will trigger failure [28]. Performance-based design methods such as the Newmark [29] sliding-block model utilise this critical acceleration value in order to make displacement predictions for specific ground motions.

Figure 8 shows that prior to the critical acceleration being reached, the wall exhibited a total displacement at the wall top of 37 mm. This comprised ~ 33 mm (or roughly 90%) due to rotation of the wall and only ~ 4 mm (about 10%) due to sliding. In the final shaking stage, when 0.5g base acceleration was applied, sliding of the wall increased significantly and reached ~ 27 mm or about 13 % of the total displacement of 195 mm. These final values should be treated with caution because of the testing limitations mentioned above.

The dominance of overturning over sliding failure modes during seismic excitation has been shown in other scale model testing with FHR facing [3, 15, 26] as well as flexibly-faced models [16] on the shake-table. But there have been limited case studies of GRS failures in the field after major-earthquake events. Tatsuoka [1] reported on one GRS wall with FHR facing, 6.2 m high and supporting a railway. During the 1995 Kobe earthquake, the wall was subjected to an estimated PGA of 0.7g. Inspection revealed overturning of approximately 260 mm and sliding of 100 mm; a higher sliding component than that recorded in Test-6. Other GRS walls in the vicinity reported limited damage.

Such comparisons between limited field data and model scale behaviour should be made in the context of appropriate scaling. That is, at the large strains induced by failure, scaling laws become invalid, and actual deformations at model scale are not comparable with those at full-scale [24]. But with correct scaling, and with small strains prior to failure, the actual mechanisms observed at model scale should be reasonably equivalent to those in the field.

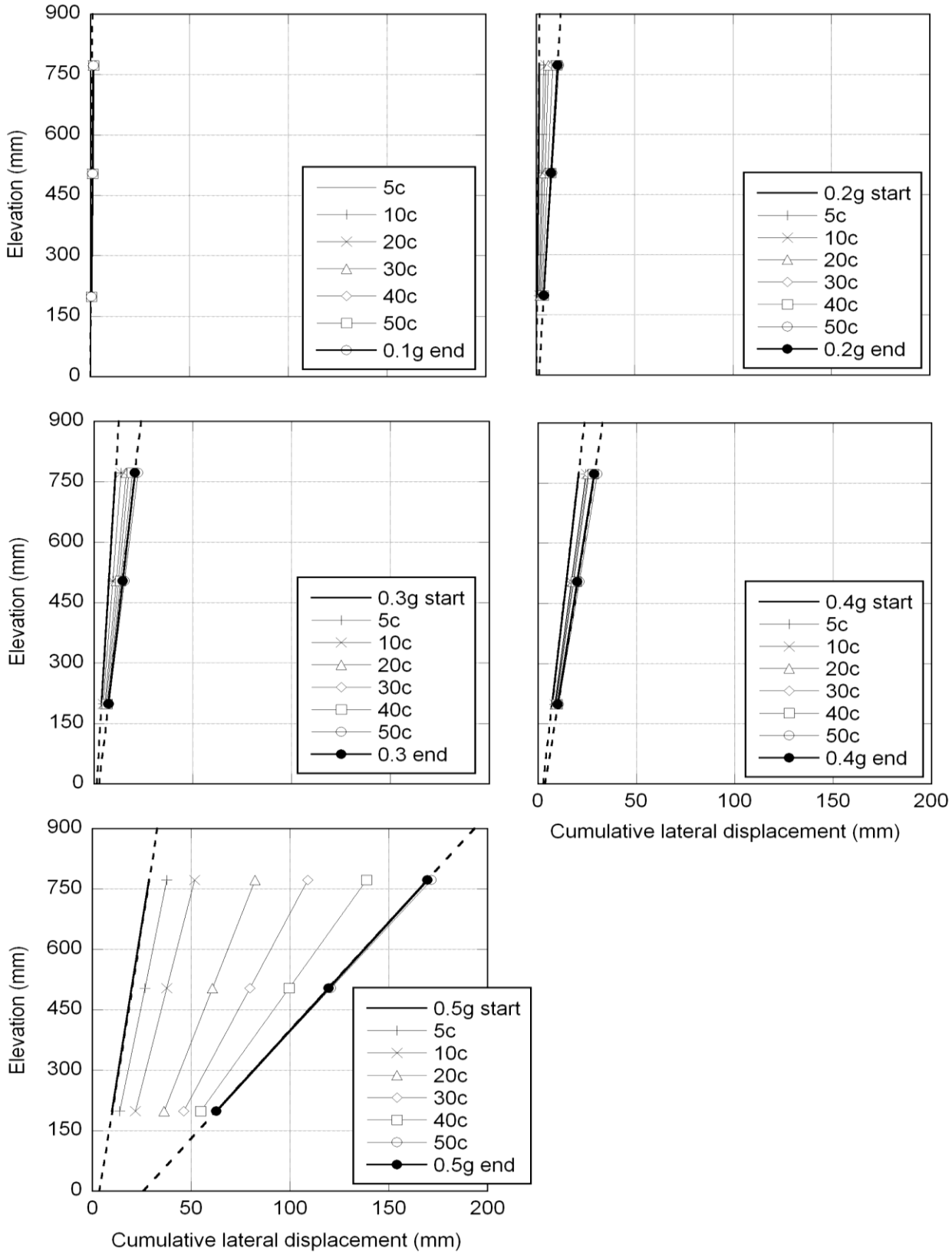

Figure 7: ***Progression of displacement recorded at the wall face during testing of Test-6. NB: "c" denotes the cycles completed.***

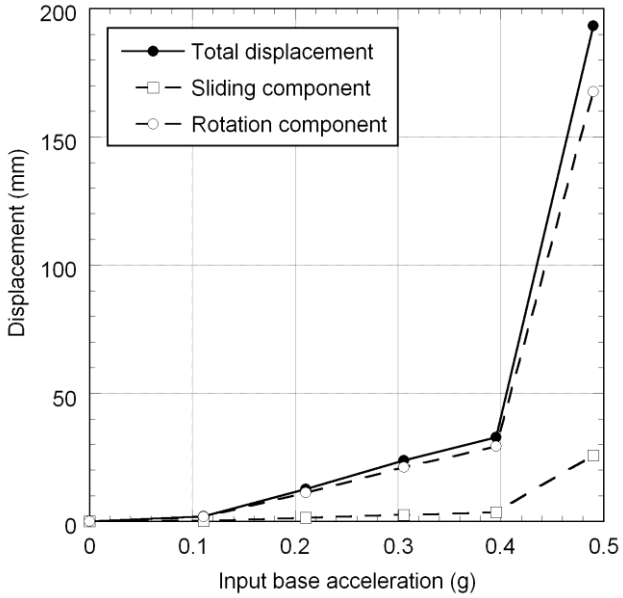

*Figure 8: **Rotation and sliding components of cumulative residual horizontal displacement of the wall top with increasing base input acceleration. Reinforced at L/H = 0.60 (Test-6). Note that the input base acceleration was calculated using the average double amplitude method.***

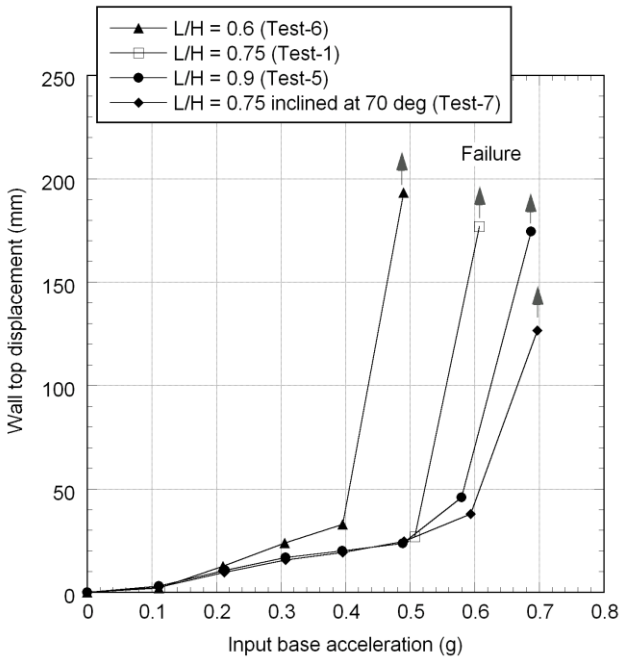

*Figure 9: **Displacement-acceleration curves for Tests-1, 5, 6 and 7. Note that Test-1 data prior to 0.5g is not plotted because the movement of the wall face was hampered by a brittle seal with the strong-box sidewall.***

Parametric study

The displacement-acceleration curves for Tests-1, 5, 6 and 7 are shown in Figure 9, revealing similar bi-linear behaviour to Test-6. The comparison also demonstrates the performance benefits gained with an increase in L/H ratio from 0.6 to 0.9, whereby the residual deformation at low levels of acceleration was generally less for L/H greater than 0.75 in comparison with L/H of 0.6, and the acceleration to cause failure increased with L/H. Regarding Figure 9, for L/H of 0.6, it appears that a greater proportion of rotation before complete failure occurred in comparison to the other tests, which may account for its greater pre-failure deformation. It can be seen in Figure 9 that there are also performance benefits in reducing the wall inclination from the vertical with an increase in the acceleration required to cause failure.

DEFORMATION OBSERVED USING PARTICLE IMAGING VELOCIMETRY (GEOPIV)

General

Images from the high speed cameras were analysed using GeoPIV, Particle Image Velocimetry software developed for geotechnical applications [6]. High-speed images of two regions were captured, however only the results from Camera 2 will be discussed in this paper. The region under analysis is approximately 650 mm tall and 250 mm wide. It is located 450 mm from the wall face, and 250 mm above the base of the model, as shown in Figure 5(a).

The GeoPIV technique divides the first image of each test into a grid of 'patches' sized a certain number of pixels, and then traces each patch through successive images by texture recognition (also known as Digital Image Correlation, DIC). In this way, the displacement of each patch during shaking can be recorded allowing shear strains within the backfill to be calculated. Details of the camera, imaging parameters, the GeoPIV technique and its validation, are presented in Appendix 1.

Displacements within the test window accumulated during Test-6 shaking are illustrated in Figure 10. The initial positions of reinforcement layers R2, R3, and R4, are also shown at the elevations of 300 mm, 450 mm and 600 mm respectively. Minimal patch displacement was recorded during the 0.1g shaking step; a steady increase in soil displacement is, however, visible with increasing base input acceleration. Within the retained backfill, the displacement is seen to be concentrated above an inclined line from reinforcement R2, whereas displacement within the reinforced soil block appears to be more horizontal. This displacement pattern is consistent with the rotational movement described in Figures 5 to 8. Note that the 0.5g shaking step is not plotted because during failure, patches moved either outside of the window or deformed so much that they could not be recognised by the software.

The progression of residual maximum shear strain, accumulated by the completion of 0.1g, 0.2g, 0.3g and 0.4g shaking steps is plotted in Figure 11. Colour contours are used to denote percentage values of localised strain. Localised cumulative shear strains up to around 20% can be identified by the completion of the 0.2g shaking step, with a shear surface from the second reinforcement layer (R2) inclined upwards into the retained backfill. Similar values of shear strain are visible at the ends of reinforcement layers R3 and R4 indicating initiation of localised deformation along the interface between the reinforced soil block and the backfill. Further shaking at 0.3g and 0.4g contributed to increasing shear strains up to 50%, along previously well-defined shear surfaces. In addition, large localized deformation is seen developing along the vertical section coinciding with the location of the ends of reinforcement layers. These images clearly show the spatial and temporal development of localized deformation including soil-reinforcement interaction. effects, and enhance the understanding of the failure mode and its evolution described in Figure 6.

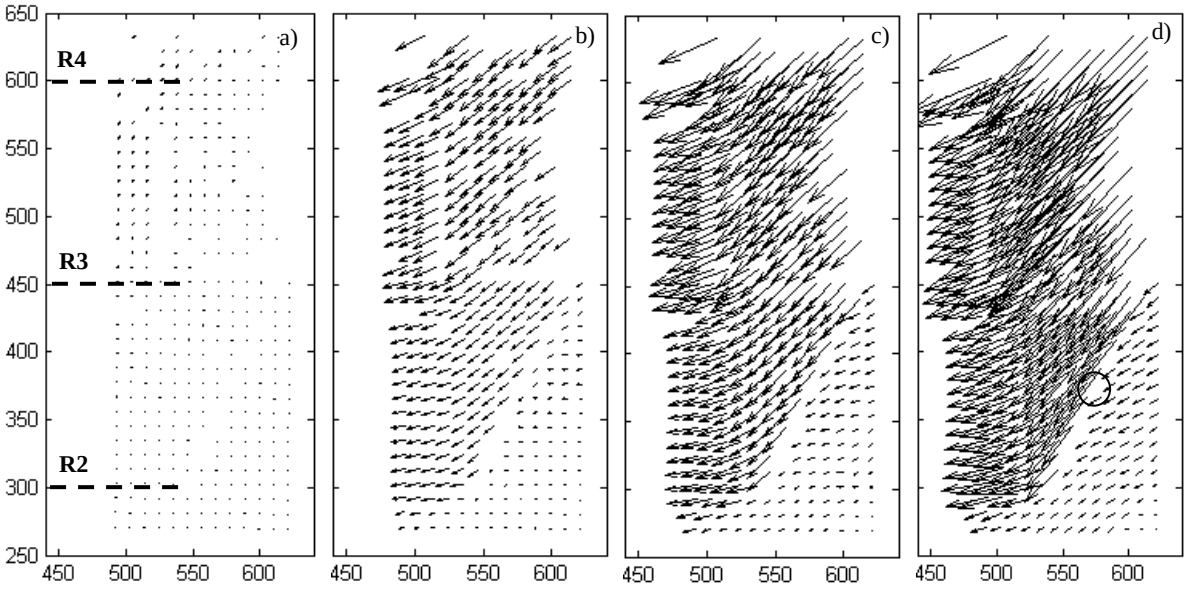

Figure 10: ***Displacement plot of imaging region for shaking steps (a) 0.1g, (b) 0.2g, (c) 0.3g and (d) 0.4g. (Note vectors have been scaled up by 3). Plots show the extent of the imaging region in millimetres from the wall toe. R4, R3 and R2 are used to denote the original position of the 4th, 3rd and 2nd reinforcement layers, respectively.***

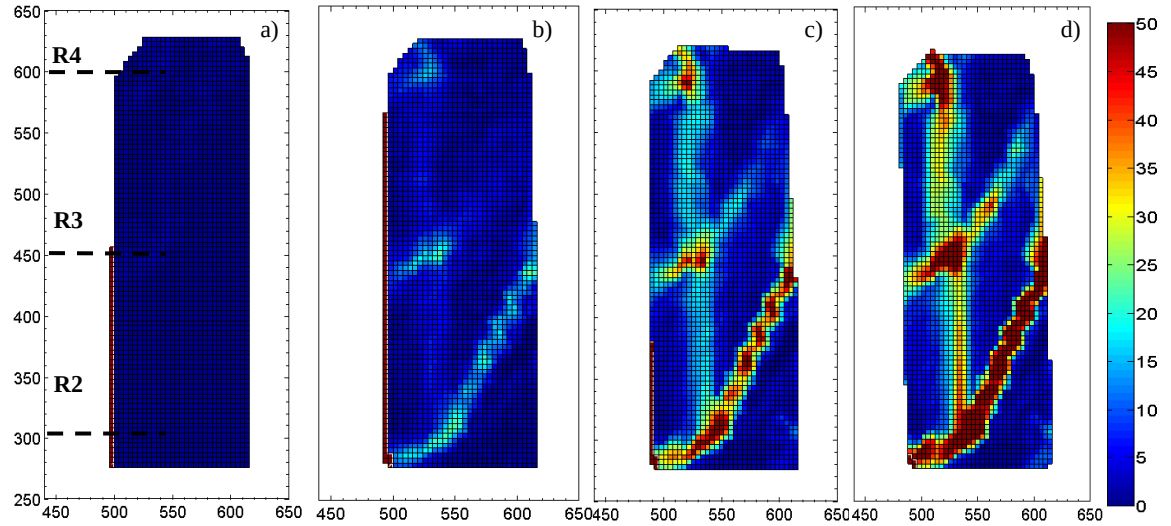

Figure 11: ***Residual shear strain of the imaging region of Test-6 reinforced with L/H = 0.6 and accumulated by the completion of: (a) 0.1g, (b) 0.2g, (c) 0.3g and (d) 0.4g shaking steps. The plotting region is the extent of the imaging region in millimetres from the wall toe.***

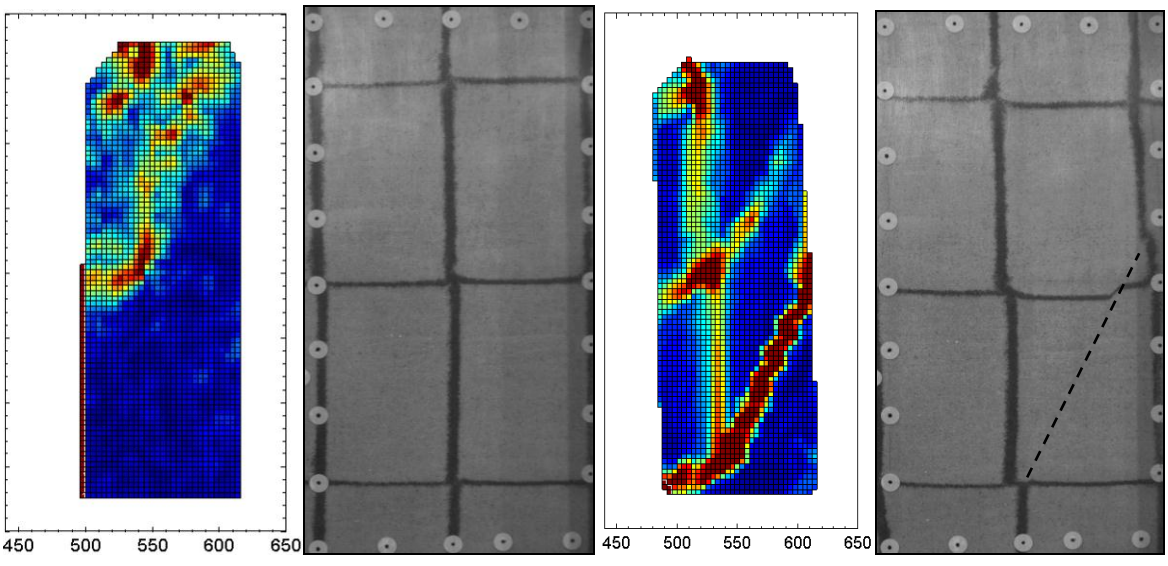

Figure 12: ***Comparison of location of failure surfaces plotted and seen within the image after (a) 0.1g and (b) 0.4g. Note that the maximum strains plotted are (a) 2% and (b) 50%.***

The progression of residual maximum shear strain, accumulated by the completion of 0.1g, 0.2g, 0.3g and 0.4g shaking steps is plotted in Figure 11. Colour contours are used to denote percentage values of localised strain. Localised cumulative shear strains up to around 20% can be identified by the completion of the 0.2g shaking step, with a shear surface from the second reinforcement layer (R2) inclined upwards into the retained backfill. Similar values of shear strain are visible at the ends of reinforcement layers R3 and R4 indicating initiation of localised deformation along the interface between the reinforced soil block and the backfill. Further shaking at 0.3g and 0.4g contributed to increasing shear strains up to 50%, along previously well-defined shear surfaces. In addition, large localized deformation is seen developing along the vertical section coinciding with the location of the ends of reinforcement layers. These images clearly show the spatial and temporal development of localized deformation including soil-reinforcement interaction effects, and enhance the understanding of the failure mode and its evolution described in Figure 6.

To better scrutinise maximum shear strain accumulated within the 0.1g shaking step, Figure 11 (a) is re-plotted using a finer scale in Figure 13. With a finer shear strain scale, the deformation by the completion of 0.1g shaking step is clearly visible, with maximum shear strains up to 2% along a shear surface from reinforcement R3 and inclined upwards into the backfill.

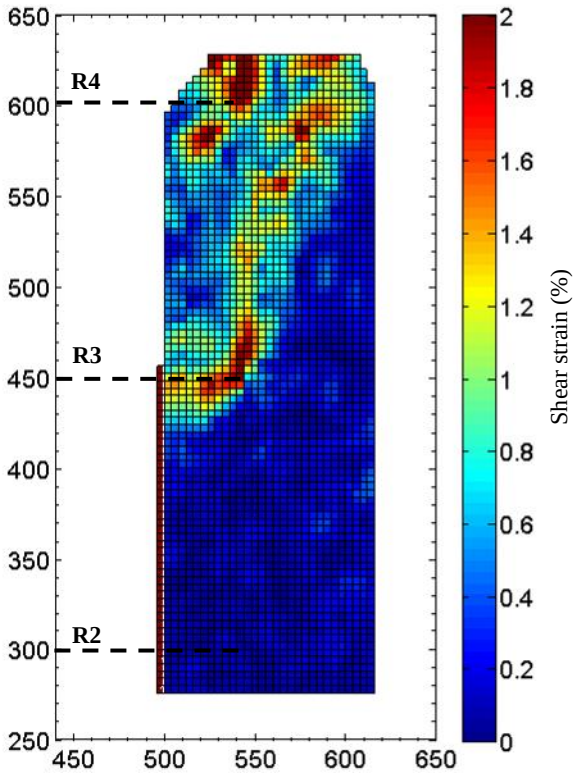

Figure 13: ***Residual shear strain accumulated by the completion of 0.1g (re-plotted at a finer scale for better visualisation) of the reinforced/retained backfill interface of Test-6 reinforced with L/H = 0.6.***

Summary of GeoPIV Analysis

The GeoPIV analysis shows the progressive development of deformation within the reinforced and retained backfill after 0.1g shaking, prior to this becoming obvious using the coloured sand lines at 0.3g. In particular, GeoPIV allowed the identification of:

- High shear strain being developed at the ends of the reinforcement layers, a localised weakness likely due to the difference in the relative stiffness between the reinforcement and backfill and their incompatible modes of deformation/movement.
- Inclined shear surfaces that propagate from the ends of the reinforcement layers upwards and into the retained backfill.
- Horizontal and inclined shear surfaces that propagate from the ends of the reinforcement layers into the reinforced soil block, contributing to the 'simple shear' deformation.
- A sub-vertical shear surface which formed behind the reinforced soil block, developing progressively downwards with the further development of inclined failure surfaces.

The deformation mechanisms observed have important ramifications to design. Firstly, they agree with and support the two-wedge model shown in Figure 2. Secondly, as rotation-induced displacement was the predominant mode of movement, with displacement accrued during low-level shaking prior to the critical acceleration being reached, this initial deformation and failure mode should be incorporated into performance-based design methods, currently based on an assessment of standard sliding block models only. Thirdly, in such models, the reinforced soil block is assumed perfectly rigid, while in reality, it was observed to undergo significant deformation in the current, and previous model-scale experiments [15, 16].

CONCLUSIONS

Seven scale model GRS walls with a FHR panel facing were tested on the shake-table at the University of Canterbury, with high-speed imaging undertaken to observe deformation within the reinforced and retained backfill. The models were 900 mm high, backfilled with Albany sand of relative density 90% and reinforced with 5 layers of stiff Microgrid reinforcement. These details were representative of GRS walls with FHR facing for the observation of deformation patterns and ultimate failure. Important design parameters such as the L/H ratio and wall inclination were varied across the testing series, and allowed the following conclusions to be made:

- An increase in the L/H ratio, or a decrease in wall inclination from the vertical to 70° to the horizontal, increased the critical acceleration required for triggering failure of the GRS wall. This also resulted in reduced deformation at low levels of acceleration.
- Deformation prior to, and during failure was predominantly by overturning, with relatively small contribution of sliding. This was accompanied by inclined shear planes which formed within the retained backfill and reinforced soil block.
- The general pattern of progressive deformation was shown using both sand markers and GeoPIV. GeoPIV was found to be able to accurately quantify the progressive development of strains previously not visible by eye, and at low levels of shaking.

APPENDIX 1: DETAILS OF GEOPIV TECHNIQUE

As shown above, the GeoPIV data collection process allowed essential information such as the location and timing of formation of shear surfaces within the backfill, and the magnitude of local strains to be obtained. This section describes the camera setup, imaging parameters, and the analysis techniques employed in more detail.

Two regions were imaged, however only the results from Camera 2 are described in this paper. Camera 2 was a

MotionPro X3 (Redlake) with a high-speed Nikkor lens (to ensure sufficient light for texture tracking). The nature of high-speed photography necessitated the storage of recorded images within the camera RAM during testing. Hence RAM constrained the frame rate, resolution and the duration of image acquisition. The monochrome camera was set with a resolution of 1,280 x 1,024 pixels, 200 frames per second frame rate, a 5 ms exposure and a total acquisition time of 12 seconds.

High-speed images taken during testing were analysed with GeoPIV software [23]. The GeoPIV method first divides an initial image into a mesh of 'patches', sized a certain number of pixels, and the texture (pattern of light and dark) of each patch is recorded. Using pattern-matching algorithms, each patch can then be traced within successive images, to determine the displacement between them. Strains within the soil mass were able to be deduced from successive images obtained from the high speed cameras over time. Marketos and Madhabushi [22] have used this method in shake table tests on model conventional retaining walls, albeit at a scale that encompassed the whole model and with resultantly less detail.

In order to transform the sand patch displacements recorded within the image (i.e. measured in terms of pixels) to real displacements measured in terms of the physical model (i.e. mm), reference grids (circular markers) placed on the inside of the transparent Perspex window and a photogrammetric transformation process are used. Photogrammetry allows the correct scaling of the image displacements, since a single scale factor cannot be used due to the spatial variation caused by factors such as: the camera and object planes not being coplanar; radial and tangential lens distortion; refraction through the viewing window [6]; and here, movement of the shake-table. A calibration sheet consisting of precisely and accurately sized and positioned dots was used to position the reference grid prior to testing, which in turn, was used to transform soil displacements measured within the image into real displacements, using GeoPIV. The reference grids also allowed the underlying shake-table motion to be separated from the motion of the Albany Sand behind the Perspex window for displacement and strain analysis.

GeoPIV calculates shear strain based on the relative displacement of patches within the backfill (the movement of the shake-table is removed as described above). For instance, one of the displacement vectors is circled in Figure 10 (d). Its length after the 0.4g shaking step is 12.9 mm (note that each vector in Figure 10 has been scaled by 3). In contrast, one vector below measures only 3.7 mm displacement. Hence the differential displacement between these two vectors is 9.2 mm, and represents a simple shearing surface across two patches, defined in Equation 1.

$$\gamma_{xy} = \frac{\Delta\delta}{t} \tag{1}$$

where γ_{XY} = shear strain in the xy-plane;
$\Delta\delta$ = the differential displacement; and
t = thickness (i.e. one patch width).

GeoPIV determines the maximum shear strain between proximate patches more precisely by linking the centroid of each patch with an extensible "element". The maximum shear strain within the soil is then calculated from the relative extension and compression of elements linking adjacent patches as in Equation 2. These values of shear strain were used in Figures 11 through 13.

$$\gamma = \sqrt{(\varepsilon_y - \varepsilon_x)^2 + \gamma_{xy}^2} \tag{2}$$

where γ = is the maximum shear strain;
ε = normal strains in the x and y directions; and
γ_{XY} = shear strain in the xy-plane.

White *et al.* [23] evaluated the precision of the GeoPIV programme in a series of physical experiments on a micro-metered translating bed of non-deforming sand. The experiments showed that the precision is a strong function of patch size (i.e. the larger the patch the greater the precision), and a weak function of image content (i.e. patches of low texture are more difficult to locate precisely than high texture patches).

In the current experiments, images from which may be considered to be of an intermediate texture, GeoPIV analysis was first conducted with three different patch sizes and spacings, 64 × 64 pixels, 32 × 32 pixels and 16 × 16 pixels to test which patch size was best suited for further analysis. In this paper, the spacing between successive patches was kept the same as the patch size, i.e. no overlap between patches. The analysis using the largest patch size did not enable sufficient detail within the image to be examined, while the smallest patch size was too small to accurately and consistently track patches. Hence patches sized 32 × 32 pixels at 32 pixel spacing were selected for the analyses presented here.

ACKNOWLEDGEMENTS

Reconnaissance of the Canterbury earthquakes was undertaken by the first author as a member of the Earthquake Commission Land Damage and Assessment Team. The first author was also supported by the Earthquake Commission (EQC) of New Zealand via postgraduate study award 6UNI/575. The financial support of the University of Canterbury and the assistance of Messrs. John Maley and Siale Faitonotu in development of the experimental apparatus are also highly appreciated.

REFERENCES

1 Tatsuoka, F. (2008). "Geosynthetic-reinforced soil structures: A cost-effective solution combining two engineering disciplines", *19th Carillo Lecture - Mexican Society for Soil Mechanics*, Aguascalientes, Mexico.

2 Federal Highways Administration (FHWA) (2001). "Mechancially Stabilized Earth Walls and Reinforced Soil Slopes Design and Construction Guidelines".

3 El-Emam, M.M. and Bathurst, R.J. (2004). "Experimental Design, Instrumentation and Interpretation of Reinforced Soil Wall Response Using A Shaking Table", *International Journal of Physical Modelling in Geotechnics*, **4**, 13-32.

4 Fairless, G.J. (1989). "Seismic Performance of Reinforced Earth Walls," Department of Civil Engineering, University of Canterbury, Christchurch.

5 Jones, C.J.F.P. (1996). "Earth reinforcement and soil structures", Thomas Telford, London.

6 White, D.J. and Take, W.A. (2002). "GeoPIV: Particle Image Velocimetry for use in geotechnical engineering", Cambridge University Engineering Department, Cambridge.

7 Murashev, A.K. (2003). "Guidelines for Design and Construction of Geosynthetic-Reinforced Soil Structures", Transfund New Zealand.

8 Murashev, A.K. (1998). “Design and construction of geosynthetic-reinforced soil structures in New Zealand”, Transfund New Zealand.

9 Sandri, D. (1997). “Performance summary of reinforced soil structures in the Greater Los Angeles area after the Northridge earthquake”, *Geotextiles and Geomembranes*, **15**(4-6), 235-253.

10 Ling, H.I., Leshchinsky, D. and Chou, N.N.S. (2001). "Post-earthquake investigation on several geosynthetic-reinforced soil retaining walls and slopes during the Ji-ji earthquake of Taiwan. *Soil Dynamics Earthquake Engineering* **21,** 297-313.

11 Stevens, G. (2011). “Observations on the effects of the Christchurch Earthquake on structures incorporating Geosynthetic and Mesh Reinforcement”, *New Zealand Geomechanics News*, **81**, 68 - 72.

12 Cubrinovski, M., Bradley, B., Wotherspoon, L., Green, R., Bray, J., Wood, C., Pender, M., Allen, J., Bradshaw, A., Rix, G., Taylor, M., Robinson, K., Henderson, D., Giorgini, S., Ma, K., Winkley, A., Zupan, J., O'Rourke, T., DePascale, G. and Wells, D. (2011). “Geotechnical Aspects of the 22 February 2011 Christchurch earthquake”, *Bulletin of the New Zealand Society of Earthquake Engineering*, **44**(4), 205-226.

13 El-Emam, M.M. and Bathurst, R.J. (2005). "Erratum: Facing contribution to seismic response of reduced-scale reinforced soil walls”, *Geosynthetics International* **12**(5), 215-238.

14 El-Emam, M.M. and Bathurst, R.J. (2007). "Influence of reinforcement parameters on the seismic response of reduced-scale reinforced soil retaining walls", *Geotextiles and Geomembranes*, **25**(1), 33-49.

15 Watanabe, K., Munaf, Y., Koseki, J., Tateyama, M. and Kojima, K. (2003). "Behaviors of several types of model retaining walls subjected to irregular excitation", *Soils and Foundations*, **43**(5), 13-27.

16 Sabermahani, M., Ghalandarzadeh, A. and Fakher, A. (2009). "Experimental study on seismic deformation modes of reinforced soil-walls", *Geotextiles and Geomembranes*, **27**, 121-136.

17 Nova-Roessig, L. and Sitar, N. (2006). "Centrifuge model studies of the seismic response of reinforced soil slopes", *Journal of Geotechnical and Geoenvironmental Engineering*, **132**(3), 388-400.

18 Izawa, J. and Kuwano, J. (2008). “Centrifuge shaking table tests on saturated reinforced soil walls”, *Proceeding of the 4th Asian Regional Conference on Geosynthetics* **1**:191-196.

19 Howard, R., Kutter, B. and Siddharthan, R. “Seismic deformation of reinforced soil centrifuge models”, *Geotechnical Earthquake Engineering and Soil Dynamics III*, University of Washington, Seattle, Washington, USA.

20 Zornberg, J. G. and Arriaga, F. (2003). “Strain distribution within geosynthetic-reinforced slopes”, *Journal of Geotechnical and Geoenvironmental Engineering*, **129**(1), 32-45.

21 Watanabe, K., Koseki,J. and Tateyama M. (2005). “Application of High-Speed Digital CCD Cameras to Observe Static and Dynamic Deformation Characteristics of Sand”, *Geotechnical Testing Journal*, Vol. **28**, No. 5.

22 Marketos, G. and Madabhushi, S.P.G. (2004). “An investigation of the failure mechanism of a cantilever retaining wall under earthquake loading”, *International Journal of Physical Modelling in Geotechnics*, **4**, 33-44.

23 White, D.J., Take, W.A. and Bolton, M.D. (2003). “Soil Deformation measurement using particle image velocimetry (PIV) and photogrammetry”, *Geotechnique*, **3**(7), 619 - 631.

24 Iai, S. (1989). “Similitude for shaking table tests on soil-structure-fluid model in 1g gravitational field”, *Soils and Foundations*, **29**(1), 105-118.

25 Jackson, P. (2010). “An Investigation into the deformation behaviour of geosynthetic reinforced soil walls under seismic loading”, **ME** thesis, University of Canterbury, Christchurch.

26 Matsuo, O., Yokoyama, K. and Saito, Y. (1998). “Shaking table tests and analyses of geosynthetic-reinforced soil retaining walls”, *Geosynthetics International*, **5**, 97 - 126.

27 Bowman, E.T., Jackson, P., Cubrinovski, M., Fannin, R.J., (2011). “Progressive failure and shear band development within model-scale reinforced soil walls subject to seismic shaking”, *Géotechnique Letters*, **1**, 53 - 57.

28 Richards, R., Jr. and Elms, D. G. (1979). “Seismic behaviour of gravity retaining walls”, *J. Geotechnical Engineering.* Div., **105**(4), 449–469.

29 Newmark, N.M., (1965). Effects of Earthquakes on Dams and Embankments”, *Géotechnique*, Vol. **15**, No. 2, pp. 139-160.